The Seventeenth International Symposium on Transport Phenomena,
4-8 September, 2006, Toyama, JAPAN

DETACHED-EDDY SIMULATION OF FLOW AROUND A CIRCULAR CYLINDER IN GROUND EFFECT

Takafumi Nishino[1], Graham T. Roberts[2] and Xin Zhang[3]

School of Engineering Sciences, University of Southampton, Southampton, SO17 1BJ, United Kingdom

ABSTRACT
In this study we performed a detached-eddy simulation (DES) of flow around a circular cylinder placed near and parallel to a moving ground, on which no boundary layer developed to interfere with the cylinder. The results were compared with experiments previously reported by the authors, and also with two-dimensional unsteady RANS computations. The DES correctly predicted the cessation of the Kármán-type vortex shedding behind the cylinder, whereas the unsteady RANS also predicted it but at a much smaller 'gap ratio' (i.e. the ratio of the gap between the cylinder and the ground, *h*, to the cylinder diameter *d*) compared with the experiments. Time-averaged force coefficients, separation angles and velocity profiles in the near wake region predicted by the DES were in good agreement with the experiments. The major features of instantaneous wake structures were well reproduced in both large- and small-gap regimes, and also in the intermediate-gap regime, where the DES predicted a temporary formation of a small dead-fluid zone behind the cylinder.

INTRODUCTION
Vortex shedding behind a circular cylinder has been the subject of a number of studies [1]. Given a long circular cylinder with its axis perpendicular to fluid flow, the well-known Kármán-type (asymmetric) vortex shedding may occur behind the cylinder, the control or suppression of which is of great interest as it is closely related to various fluid-mechanical properties of practical importance, such as flow-induced forces, vibrations and noises, and the efficiencies of heat and mass transfer. There are several situations where this type of vortex shedding may cease, and one of them is when a plane boundary or ground is located near the cylinder; the focus of the present study is on this flow configuration.

The characteristics of flow around a circular cylinder placed near and parallel to a ground are governed not only by the Reynolds number *Re* but also by the gap ratio, i.e., the ratio of the gap between the cylinder and the ground, *h*, to the cylinder diameter *d* [2]. However the mechanisms of the flow and force variations caused by different *h/d*, or 'ground effect', are in general rather complicated since they can be significantly affected by the state of the boundary layer formed on the ground [3, 4]. Hence the present authors [5] recently conducted a series of experiments on a circular cylinder placed near a moving ground running at the same speed as the freestream so as to eliminate the confusing effects of the boundary layer. As a result, the characteristics of the flow were classified into three regimes: large-gap ($h/d > 0.5$), intermediate-gap ($0.35 < h/d < 0.5$), and small-gap ($h/d < 0.35$) regimes. In the large-gap regime, large-scale Kármán-type vortices were generated just behind the cylinder, whereas in the small-gap regime, the vortex shedding ceased and instead a dead-fluid zone was created, as presented in Fig. 1 (reproduced from Ref. [5]). Also of particular interest in the study was that the drag on the cylinder rapidly decreased as *h/d* decreased from 0.5 to 0.35, but became constant for $h/d < 0.35$, the latter of which had not been observed in the earlier studies using a fixed ground.

The numerical study reported in this paper is a subsequent study of the experiments described above. Flow around a circular cylinder, however, is still a very challenging subject in itself in today's computational fluid dynamics (CFD) even if the cylinder is outside the ground effect; unsteady Reynolds-averaged Navier-Stokes (URANS) simulations cannot reproduce with sufficient accuracy the flow structures of wide-ranging spatial and time scales, whilst large-eddy simulations (LES) are possible but still quite expensive [6]. Detached-eddy simulation (DES) [7] is one of the novel approaches that combine the concepts of URANS and

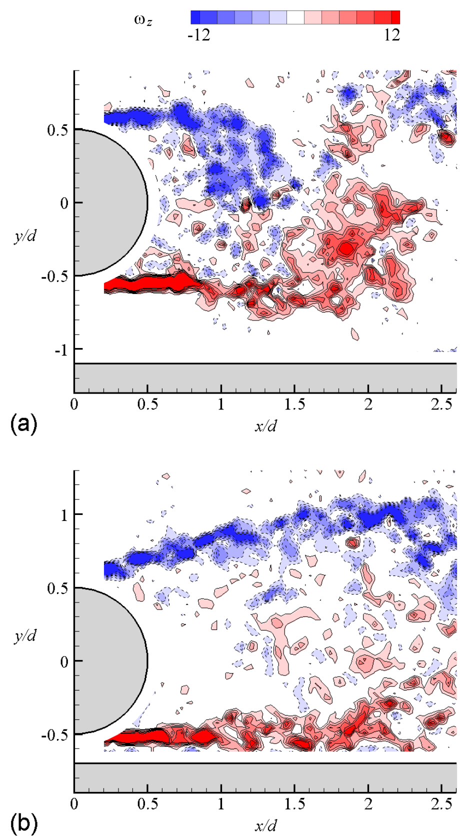

Figure 1. Typical instantaneous spanwise vorticity fields behind a circular cylinder in ground effect: (a) $h/d = 0.6$, (b) $h/d = 0.2$, measured by PIV, $Re = 4.0 \times 10^4$ (cf. Ref [5]).

---
[1] *Ph.D. Candidate, E-Mail: nishino@soton.ac.uk*
[2] *Senior Lecturer, E-mail: gtr@soton.ac.uk*
[3] *Professor, E-mail: x.zhang1@soton.ac.uk*

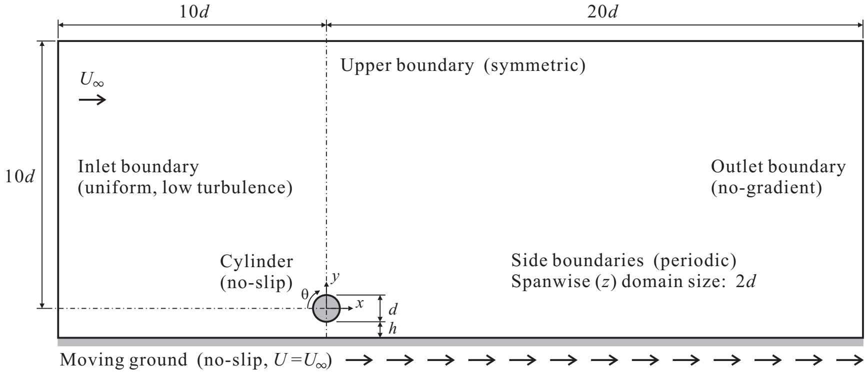

Figure 2. Computational domain and boundary conditions.

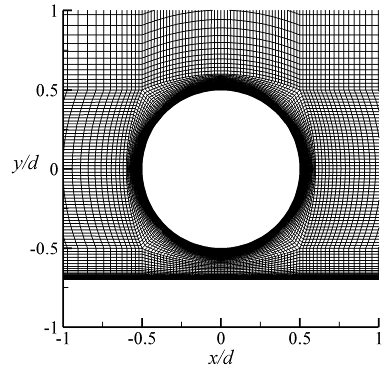

Figure 3. Computational grid (*h/d* = 0.2).

LES to obtain realistic solutions for practical high-*Re* flows at acceptable computational costs. Travin et al. [8] performed the DES of the subcritical (laminar-separation) and postcritical (turbulent-separation) flows around a circular cylinder, and showed that the results were in good agreement with experiment and also LES especially at a lower (subcritical) *Re* of 5.0×10^4.

The main objective of the present study is to show how accurately the DES can reproduce the flow around a circular cylinder in ground effect; the results of this validation may serve as a primary criterion for the applicability of DES to flows involving the problem of vortex shedding and its control or suppression. URANS simulations are also performed for the purpose of comparison; the low Reynolds number *k-ε* model of Launder and Sharma (LS *k-ε*) [9] and the Spalart-Allmaras model (S-A) [10] are employed since they are two of the most common turbulence models still widely used in both academia and industry. The discussion here is restricted to the subcritical flow (Re = 4.0×10^4, based on the cylinder diameter) to focus on the issues relevant to the ground effect.

COMPUTATIONAL DETAILS

Three-dimensional (3-D) DES and two-dimensional (2-D) URANS simulations were performed on flow around a circular cylinder placed near and parallel to a moving ground. Figure 2 shows the computational domain and boundary conditions employed in this study; the ground effect was simulated by changing the gap ratio *h/d* from 1.0 to 0.1. The computations were conducted using a commercial CFD package, FLUENT6 [11], in which a finite volume method was used to discretise governing and model equations for incompressible turbulent flows to be solved. The equations were spatially discretised with second-order accuracy on multi-block structured grids (cf. Fig. 3), temporally discretised using a second-order fully-implicit scheme, and iteratively solved with pressure correction equations derived using the SIMPLE algorithm [12]. Full details and the accuracy of the computations have been given in Ref. [13]; only the key points will be further described below.

The main feature of the DES performed in this study is that a single turbulence model (a slightly modified version of the S-A model) serves as a statistical model (URANS mode) in near-wall regions, and also serves as a subgrid-scale model (LES mode) in far-wall regions. Specifically, the nearest-wall-distance *n* that governs the eddy viscosity in the original S-A model [10] is replaced in the DES by a new length scale $\tilde{n}$ defined as

$$\tilde{n} = \min\,[n, 0.65\Delta_{\max}], \quad \Delta_{\max} = \max\,[\Delta x, \Delta y, \Delta z], \qquad (1)$$

where Δx, Δy and Δz denote the size of a control-volume in each direction. This simple and convenient formulation of the DES, however, raises an issue concerning the physical interpretation of the 'grey area' ($n \approx 0.65\Delta_{\max}$), where the mode is switched between URANS and LES, and the justification of the switch relies on the disparity of the length scales between the attached- and detached-eddies [14]. That is, the grid spacing in DES needs to be carefully decided so that the boundary layers and the separated shear layers are resolved in the URANS and LES modes, respectively. In this study the spanwise grid spacing Δz was of most importance as it governed the mode change around the cylinder; two Δz of 0.05*d* and 0.025*d* were tested in a preliminary computation, and the influence on the time-averaged drag coefficient of the cylinder was about 10% (the former was eventually adopted to save computational costs, resulting in a 3-D grid of about 1.2 million cells). The influence of other computational factors, such as the domain size, spatial resolution in the *x* and *y* directions, and time resolution, was found to be smaller than that of Δz. For the time resolution, a dimensionless time step $\Delta t \cdot U_\infty / d$ of 0.021 was eventually adopted in this study.

As concerns the inlet boundary condition, a uniform flow of very low turbulence level (corresponding to the turbulence intensity of 0.3% and the turbulent viscosity ratio of unity) was given so as to simulate the subcritical flow (Re = 4.0×10^4) and to compare the results with the experiments. For the DES, however, the so-called 'trip-less approach' was additionally used, following Travin et al. [8]. Specifically, the turbulent viscosity ratio at the inlet was reduced from unity to 10^{-9} after the flow field had sufficiently developed. The computation was then continued until the flow field had developed again, and thereafter the time-averaged data were collected over a further 100 dimensionless time periods.

RESULTS AND DISCUSSION

Mean and fluctuating forces

Figure 4 shows the time-averaged drag behaviour of the cylinder in ground effect predicted by DES (S-A based, 3-D) and URANS (LS *k-ε* and S-A, 2-D). The results of the experiments [5] are also shown in the same figure for the purpose of comparison. An important feature to be focused on here is the critical change in C_D due to the cessation of the vortex shedding: in the experiments the drag was observed to rapidly decrease as the gap ratio *h/d* decreased from 0.5 to 0.35. As can be seen from the figure, the 2-D URANS predicted the critical change in C_D but at smaller *h/d* of 0.2 to 0.1, as they 'incorrectly' predicted the large-scale vortex shedding for *h/d* of down to 0.2. Meanwhile, the drag behaviour predicted by the DES agreed better with the experiments, although the predicted values of C_D were slightly higher than the experiments for all *h/d* investigated.

Figure 5 shows the time variation of the drag and lift coefficients predicted by the DES for different *h/d*. Note that the solid and dashed lines indicate C_D and C_L, respectively. It is obvious from the figures that the DES captured the cessation of the periodic vortex shedding between two *h/d* of 0.4 and 0.3, which is consistent with the experiments. Of further interest is that the periodic shedding temporarily ceased at *h/d* = 0.4 [Fig. 5(c), at $t \cdot U_\infty / d$ of around 75], and temporarily awakened at *h/d* = 0.3 [Fig. 5(d), at $t \cdot U_\infty / d$ of around 60 and 110]. This qualitatively agrees with the experimental observation that the large-scale vortex shedding was intermittent in the intermediate-gap regime [5]; instantaneous flow fields

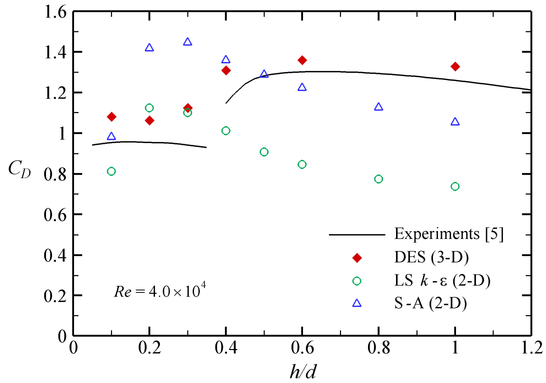

Figure 4. Time-averaged drag coefficient vs. gap ratio.

will be shown later in Fig. 12 to discuss the intermittency of the vortex shedding in more detail.

Separation angle and pressure distribution

Figure 6 shows the time-averaged separation angles on both upper (open) and bottom (gap) sides of the cylinder in ground effect predicted by the DES and URANS simulations. The results of the experiments [5] are also presented here for the purpose of comparison. Note that $|\theta_{sep}|$ plotted in this figure indicates the magnitude of the

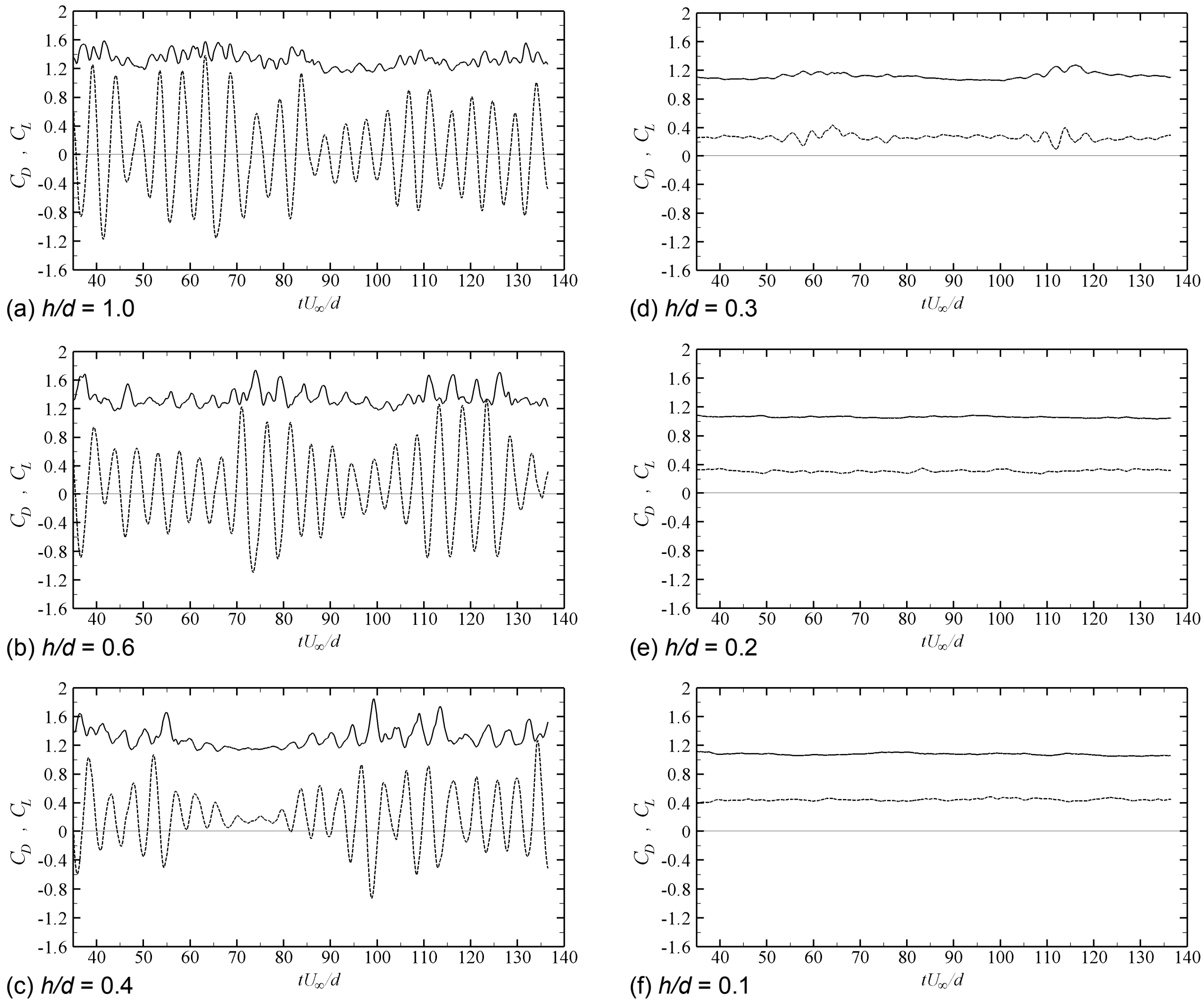

Figure 5. Time variation of drag and lift coefficients (DES); solid and dashed lines indicate C_D and C_L, respectively.

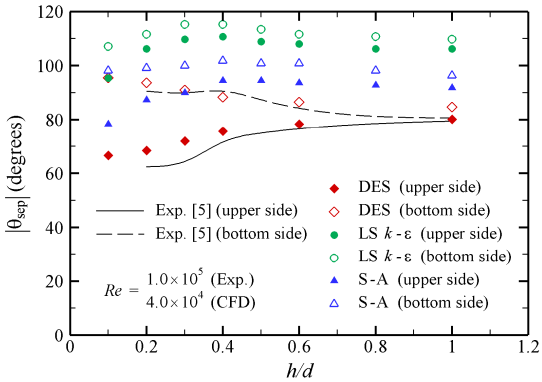

Figure 6. Time-averaged separation angle vs. gap ratio.

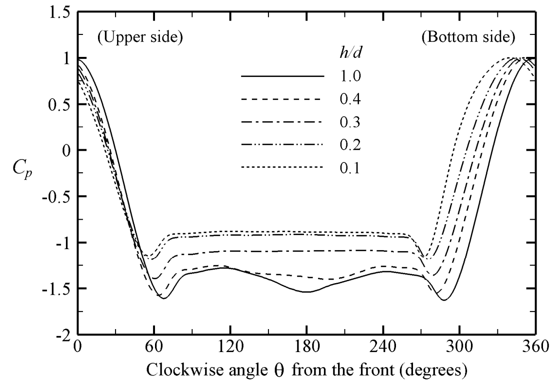

Figure 7. Time-averaged pressure distributions (DES).

angle from the front (x/d = –0.5, y/d = 0) to the separation point. It can be seen that the 2-D URANS simulations predicted much larger separation angles compared with the experiments, which is the main reason of the lower C_D predicted in the large-gap regime (cf. Fig. 4), whereas the DES agreed better with the experiments.

Figure 7 shows the mean pressure distributions around the cylinder predicted by the DES for different gap ratios. The results clearly describe the mechanisms of the drag and lift variations in ground effect, that is, the drag reduction occurs due to an increase in the base pressure, whilst the lift gradually increases as the gap decreases mainly because the stagnation point shifts to the bottom side of the cylinder. Of importance is that only small differences can be seen in the base pressure between h/d of 0.2 and 0.1, which explains the nearly constant level of drag on the cylinder in the small-gap regime. There are, unfortunately, no experimental data available on the pressure distribution for the same flow configurations to be compared with, although a good accuracy of DES on a pressure distribution around a circular cylinder in a uniform cross-flow (i.e., outside the ground effect) has been reported by Travin et al. [8] and also confirmed by the present authors.

Mean flow structure

Figure 8 shows the time-averaged streamwise velocity contours for different gap ratios. The DES predicted the recirculation region behind the cylinder to be significantly elongated as h/d decreases from 0.4 to 0.3 and lower. This agrees with the experimental results obtained using PIV [5], and explains the increase in the base pressure and hence the decrease in the drag.

Comparisons of the streamwise velocity profiles with the PIV results are given in Fig. 9 for two h/d of 0.6 and 0.2. Note that the profiles at x/d = 0.5, 1.0, 1.5, 2.0, 2.5 and 3.0 are plotted in the figure (x/d = 0.5 and 3.0 are only for the computations). It can be seen from the figure that the DES properly predicted the mean wake flows for both large- and small-gap regimes, whereas the 2-D S-A

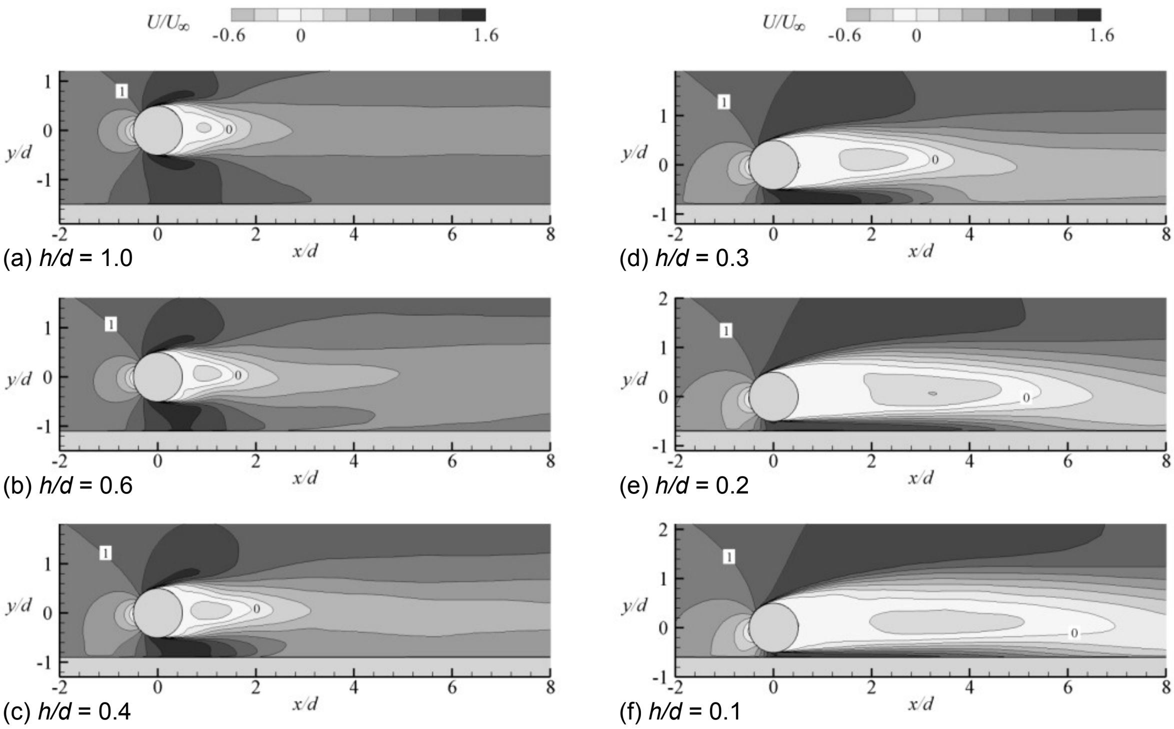

Figure 8. Contours of non-dimensional mean streamwise velocity (DES, $Re = 4.0\times10^4$).

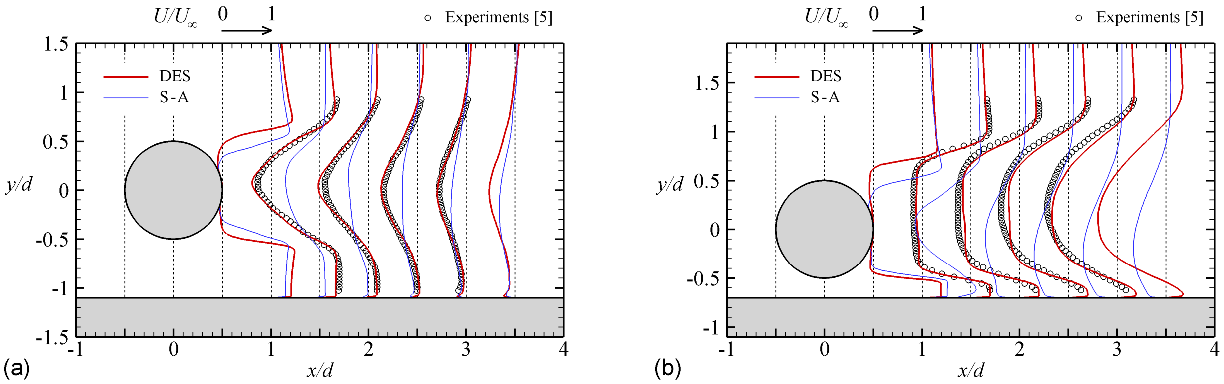

Figure 9. Mean streamwise velocity profiles for (a) *h/d* = 0.6, and (b) *h/d* = 0.2 ($Re = 4.0 \times 10^4$).

simulations failed to capture the features, especially for the small-gap regime.

Instantaneous flow structure

Figure 10 shows typical instantaneous wake structure of the cylinder in ground effect predicted by the DES. Note that the colours indicate the spanwise (z) coordinate to make visible the details of the wakes. A clear difference in the wake structure can be seen between the two gap ratios; three-dimensional large-scale vortex shedding was predicted behind the cylinder at *h/d* = 0.6, whereas two nearly parallel shear layers (but still having three-dimensional turbulent structures) were formed at *h/d* = 0.2. The mid-span sections of these two instantaneous flow fields are shown in Fig. 11(a) and (b), respectively, where the profiles of non-dimensional spanwise vorticity are plotted. A comparison with the PIV results (cf. Fig. 1) may suggest that the DES successfully captured even the instantaneous wake characteristics of the cylinder in the large- and small-gap regimes.

Another promising aspect of DES was found in the intermediate-gap regime. Figure 12 shows instantaneous spanwise vorticity fields behind the cylinder (*h/d* = 0.4) obtained at two different time instants $t \cdot U_\infty / d$ of 136.5 and 75.6. Of interest is that at $t \cdot U_\infty / d$ =75.6, around which the fluctuations of the forces almost diminished (cf. Fig. 5), the large-scale vortices were still predicted but a little away from the cylinder, resulting in a small dead-fluid zone generated behind the cylinder. This might be considered as an indication of the intermittency of the vortex shedding in the near wake region, although the rate of occurrence of the dead-fluid zone predicted in the DES seemed much lower than that observed in the PIV measurements at this gap ratio.

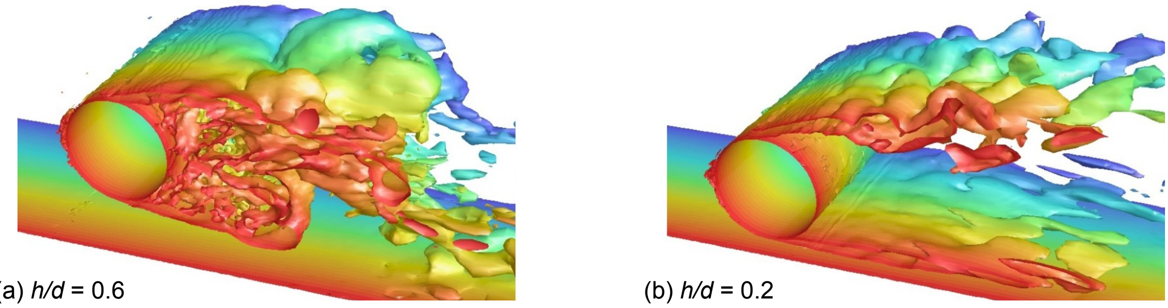

(a) *h/d* = 0.6 (b) *h/d* = 0.2

Figure 10. Isosurfaces of the magnitude of instantaneous vorticity (DES, $Re = 4.0 \times 10^4$); colours indicate the spanwise coordinate (blue: *z/d* = 0, red: *z/d* = 2).

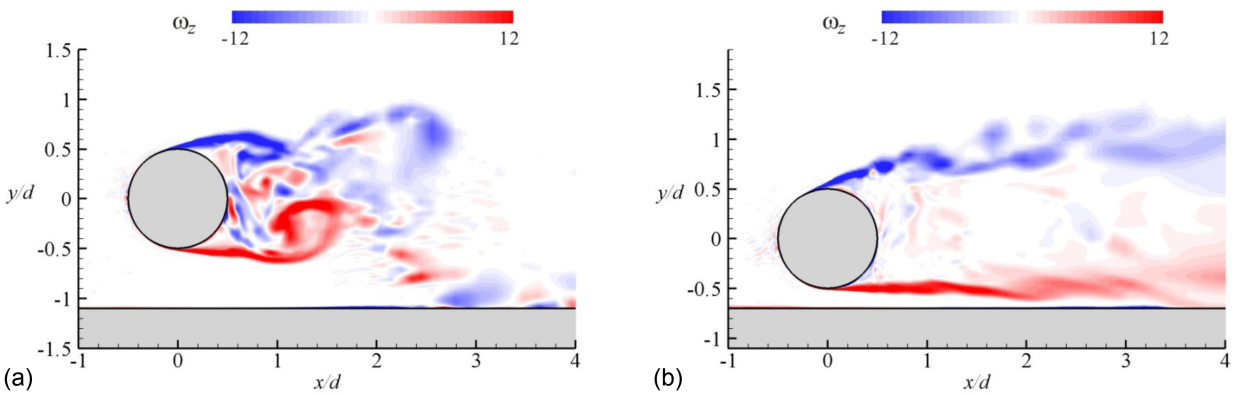

Figure 11. Typical instantaneous spanwise vorticity fields for (a) *h/d* = 0.6, and (b) *h/d* = 0.2 (DES, $Re = 4.0 \times 10^4$).

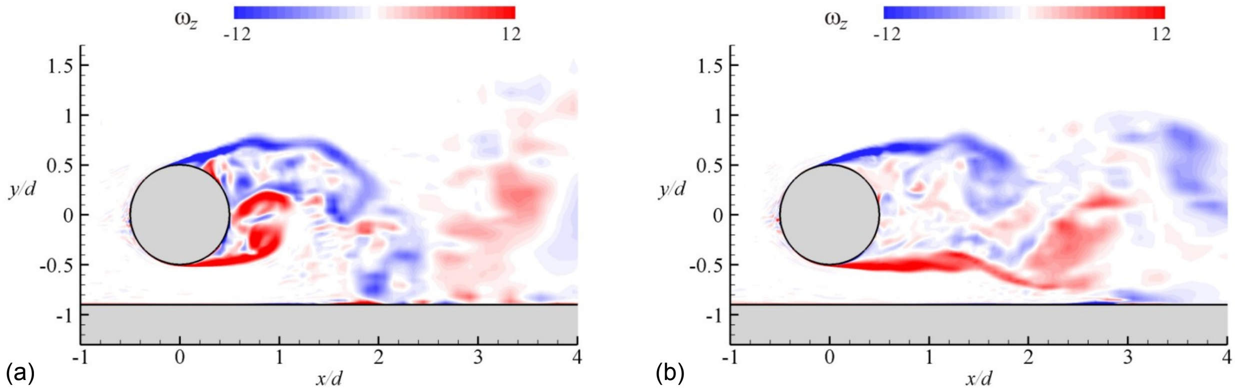

Figure 12. Instantaneous spanwise vorticity fields at two different time instants in the intermediate-gap regime: (a) $t \cdot U_\infty / d$ = 136.5, and (b) $t \cdot U_\infty / d$ = 75.6 (DES, *Re* = 4.0×10^4, *h/d* = 0.4).

CONCLUSIONS

The detached-eddy simulation of a subcritical flow (*Re* = 4.0×10^4) around a circular cylinder placed near and parallel to a moving ground was performed. The results were compared with the experiments previously reported by the authors. 2-D URANS simulations employing the LS *k-ε* and the S-A models were also performed for the purpose of comparison.

An important conclusion from this numerical study is that the DES successfully captured the critical behaviour of the flow around the cylinder in ground effect. The DES predicted the cessation of the large-scale, Kármán-type vortex shedding behind the cylinder between two gap ratios *h/d* of 0.4 and 0.3, which was consistent with the experiments, whereas the 2-D URANS also captured the critical change but at much smaller *h/d* of 0.2 to 0.1. The time-averaged force coefficients, separation angles and velocity profiles in the near wake region predicted by the DES were in good agreement with the experiments, and instantaneous vorticity fields predicted were found to be similar to those obtained from PIV measurements. These results may suggest the applicability of the DES to flows involving the problem of vortex shedding and its control or suppression in many practical applications.

ACKNOWLEDGEMENT

The work reported in this paper was supported in part by a research scholarship from the School of Engineering Sciences, University of Southampton, United Kingdom.

NOMENCLATURE

C_D	drag coefficient
C_L	lift coefficient
C_p	pressure coefficient
d	cylinder diameter, m
h	gap between cylinder and ground, m
n	nearest wall distance, m
Re	Reynolds number
t	time, s
U, V, W	Cartesian components of velocity, m/s
U_∞	freestream velocity, m/s
x, y, z	Cartesian coordinates, m
$\Delta x, \Delta y, \Delta z$	size of control-volume, m
θ	angle, degrees
θ_{sep}	separation angle, degrees
ω_z	non-dimensional spanwise vorticity, $(\partial V/\partial x - \partial U/\partial y)\, d/U_\infty$

REFERENCES

1. M.M. Zdravkovich, *Flow around Circular Cylinders: Vol 1: Fundamentals*, Oxford University Press, Oxford, UK (1997).
2. P.W. Bearman, M.M. Zdravkovich, “Flow around a Circular Cylinder near a Plane Boundary”, *J. Fluid Mech.*, Vol. 89, pp. 33-47 (1978).
3. M.M. Zdravkovich, “Forces on a Circular Cylinder near a Plane Wall, *Applied Ocean Research*, Vol. 7, pp. 197-201 (1985).
4. C. Lei, L. Cheng, K. Kavanagh, “Re-Examination of the Effect of a Plane Boundary on Force and Vortex Shedding of a Circular Cylinder”, *J. Wind Eng. Ind. Aerodyn.*, Vol. 80, pp. 263-286 (1999).
5. T. Nishino, G.T. Roberts, X. Zhang, “An Experimental Study of Flow around a Circular Cylinder with and without End Plates in Ground Effect”, AIAA Paper 2006-3551, *Proc. of the 36th AIAA Fluid Dynamics Conference and Exhibit*, 5-8 June, San Francisco, CA, USA (2006).
6. P.R. Spalart, “Strategies for Turbulence Modelling and Simulations”, *Int. J. Heat Fluid Flow*, Vol. 21, pp. 252-263 (2000).
7. M. Shur, P.R. Spalart, M. Strelets, A. Travin, “Detached-Eddy Simulation of an Airfoil at High Angle of Attack”, *Engineering Turbulence Modelling and Experiments 4*, eds. W. Rodi and D. Laurence, Elsevier, Oxford, UK, pp. 669-678 (1999).
8. A. Travin, M. Shur, M. Strelets, P. Spalart, “Detached-Eddy Simulations Past a Circular Cylinder”, *Flow, Turb. Comb.*, Vol. 63, pp. 293-313 (2000).
9. B.E. Launder, B.I. Sharma, “Application of the Energy-Dissipation Model of Turbulence to the Calculation of Flow near a Spinning Disc”, *Lett. Heat Mass Transfer*, Vol. 1, pp. 131-137 (1974).
10. P.R. Spalart, S.R. Allmaras, “A One-Equation Turbulence Model for Aerodynamic Flows”, AIAA Paper 92-0439 (1992).
11. Fluent Inc., *Fluent 6.2 User's Guide*, Fluent Inc., Lebanon, NH, USA (2005).
12. S.V. Patankar, *Numerical Heat Transfer and Fluid Flow*, Hemisphere Publishing Corporation, WA, USA. (1980).
13. T. Nishino, “An Investigation of Flow around a Circular Cylinder in Ground Effect”, MPhil/PhD Transfer Thesis, School of Engineering Sciences, University of Southampton, UK (2006).
14. P.R. Spalart, “Young-Person's Guide to Detached-Eddy Simulation Grids”, NASA/CR-2001-211032, Langley Research Center, National Aeronautics and Space Administration (NASA), Virginia, USA (2001).